

# Skyrmion crystals in the triangular Kondo lattice model

Zhentao Wang<sup>1,2</sup> and Cristian D. Batista<sup>2,3</sup>

<sup>1</sup> School of Physics and Astronomy, University of Minnesota, Minneapolis, Minnesota 55455, USA

<sup>2</sup> Department of Physics and Astronomy, The University of Tennessee, Knoxville, Tennessee 37996, USA

<sup>3</sup> Quantum Condensed Matter Division and Shull-Wollan Center, Oak Ridge National Laboratory, Oak Ridge, Tennessee 37831, USA

July 19, 2022

## Abstract

We present a systematic study of the formation of skyrmion crystals in a triangular Kondo Lattice model for generic electron filling fractions. Our results demonstrate that the four-sublattice chiral antiferromagnetic ordering that was reported more than one decade ago can be understood as the dense limit of a sequence of skyrmion crystals whose lattice parameter is dictated by the Fermi wave-vector. Moreover, the skyrmion crystals remain stable at zero temperature even in absence of easy-axis anisotropy when the Kondo exchange becomes larger than a critical value. This observation has important implications for the ongoing search of skyrmion crystals in metallic materials with localized magnetic moments.

---

## Contents

1	Introduction	1
2	Model and Results	3
3	Conclusion	7
A	Variational Method	8
B	Fourier analysis	10
	References	10

---

## 1 Introduction

The magnetic skyrmion crystals (SkX) envisioned by Bogdanov and Yablonskii [1, 2] were finally discovered in 2009 studying a family of chiral magnets that includes MnSi, Fe<sub>1-x</sub>Co<sub>x</sub>Si, FeGe

and  $\text{Cu}_2\text{OSeO}_3$  [3–7]. One year before that remarkable discovery, a four-sublattice chiral antiferromagnetic (AFM) ordering was reported to be present in the zero-temperature phase diagram of the triangular Kondo Lattice model (TKLM) [8]. This chiral ordering can be regarded as the dense (short wavelength) limit of a sequence of SkXs that emerge in the TKLM for general filling fractions. In the dense limit, each magnetic unit cell contains one skyrmion and the scalar spin chirality becomes uniform. As it was pointed out in previous works [8,9], the triple- $Q$  four-sublattice chiral AFM ordering is favored relative to a single- $Q$  ordering because the triple- $Q$  ordering simultaneously gaps out the independent pieces of Fermi surface that are connected by the symmetry related ordering wave vectors  $Q_1$ ,  $Q_2$  and  $Q_3$ . This argument can in principle be extended to other electron filling fractions that lead to smaller ordering wavevectors  $Q = |Q_\nu|$  due to the smaller size of the Fermi surface [see Fig. 1(a)]. Based on this observation, we can conjecture that SkXs with longer lattice constants (or wavelength) should be ubiquitous ground states of the *isotropic* TKLM for a continuous range of electron filling fractions [10].

While the conjecture is supported by an increasing number of experimental results on centrosymmetric metallic magnets [11–15], numerical studies of the KLM have only found SkXs for fine-tuned sets of Hamiltonian parameters [16]. The basic reason is that it is very challenging to obtain accurate enough numerical results for the general case. Consequently, recent theoretical studies of the SkX formation have focused on phenomenological models that assume a certain form and sign of 4-spin interactions [17], which are expected to mimic the effective spin-spin interactions generated by the KLM. Since a perturbative treatment of the Kondo exchange breaks down beyond second order at low enough temperatures [9,18], higher order spin interactions are normally incorporated in an ad-hoc manner [17] or by fitting first principles calculations [19]. Alternatively, the KLM has also been studied in the double exchange limit [20,21], where additional spin-orbit couplings were introduced to facilitate SkX formation [22,23]. Only very recently, it was demonstrated that SkXs can naturally emerge in the weak-coupling limit of the KLM for generic filling fractions and model parameters [24] if an easy-axis spin anisotropy is present. In this limit, the KLM can be reduced to the Ruderman-Kittel-Kasuya-Yosida (RKKY) model [25–27]. Away from this regime, effective higher order spin interactions become relevant, and it remains to be demonstrated that SkXs can generically emerge even in absence of easy-axis anisotropy.

The numerical challenge of obtaining a  $T = 0$  phase diagram of the KLM arises from the smallness of the effective interactions between localized moments in comparison with the bare Hamiltonian parameters. Even the small size effects associated with relatively large finite lattices can still switch the relative stability of two competing orders in comparison to the thermodynamic limit. This situation persists for a Kondo exchange interaction  $J$  comparable to the nearest-neighbor hopping  $t$ , posing a serious challenge for numerical techniques. Here we avoid these undesirable size effects by implementing a novel variational method *in the thermodynamic limit*. This method reveals that SkXs are indeed ubiquitous ground states of the *isotropic* TKLM induced by relatively large higher order spin interactions caused by the above-mentioned Fermi surface effects [10]. The field induced SkX phases emerge above a critical coupling strength  $J/t$ , implying that moving away from the strongly localized regime of  $f$ -electron magnets (RKKY limit) is important to stabilize these topological spin textures.

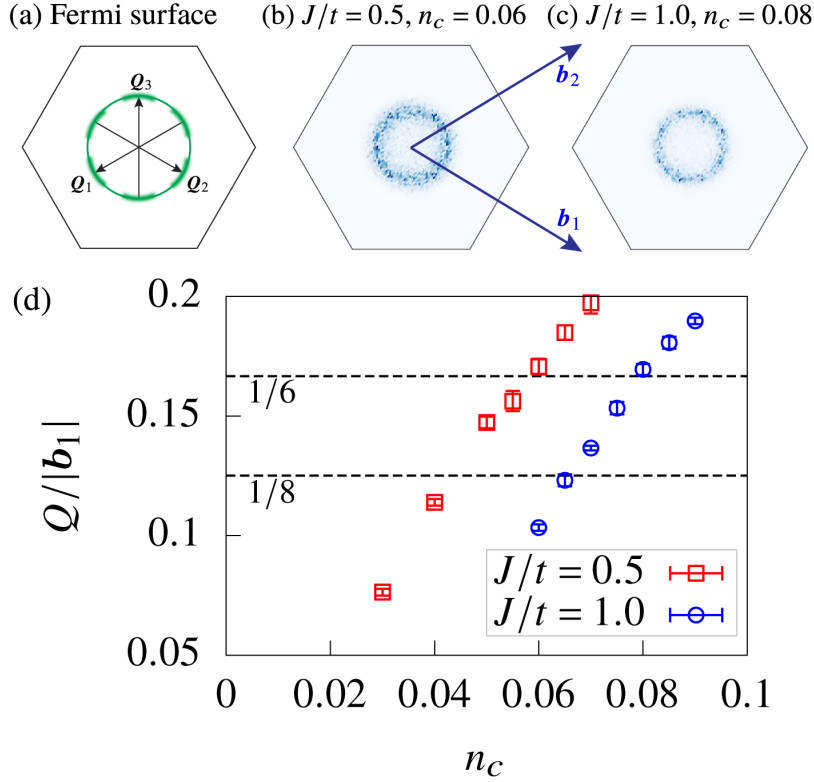


Figure 1: (a) Illustration of independent pieces of Fermi surface that are connected by the symmetry related ordering wave vectors  $\{Q_1, Q_2, Q_3\}$  at low filling fractions. (b)-(d) KPM-SLL results for the TKLM on a  $96 \times 96$  lattice with  $H = D = 0$  and  $T = 10^{-5} J^2/t$ . (b)-(c) Snapshots of the static spin structure factor  $S(q)$ .  $\{b_1, b_2\}$  are the basis vectors in the reciprocal space. (d) Ordering wave number as a function of the filling fraction.

## 2 Model and Results

We consider a 2D TKLM with *classical* local magnetic moments  $S_i$ :

$$\mathcal{H} = -t \sum_{\langle ij \rangle, \sigma} (c_{i\sigma}^\dagger c_{j\sigma} + h.c.) + J \sum_{i, \alpha\beta} c_{i\alpha}^\dagger \sigma_{\alpha\beta} c_{i\beta} \cdot S_i - H \sum_i S_i^z + D \sum_i (S_i^z)^2, \quad (1)$$

where the operator  $c_{i\sigma}^\dagger$  ( $c_{i\sigma}$ ) creates (annihilates) an itinerant electron on site  $i$  with spin  $\sigma$  and  $t > 0$ . The Kondo exchange  $J$  couples the local magnetic moments  $S_i$  to the conduction electrons ( $\sigma$  is the vector of the Pauli matrices) and  $|S_i| = 1$ . The last two terms represent a Zeeman coupling to an external field  $H$  and an easy-axis single-ion anisotropy ( $D \leq 0$ ).

We start by computing the change of the ordering wave vectors  $Q_\nu$  as a function of the electron filling fraction  $n_c$ . In the weak-coupling limit ( $J \ll t$ ), the effective spin-spin interactions are described by an RKKY Hamiltonian and the ordering wave vectors are obtained by maximizing the Lindhard function [24]. However, a different method must be used to find the values of  $Q_\nu$  away from this regime because higher order spin interactions produce a significant renormalization of the ordering wave vectors  $Q_\nu$ <sup>1</sup>.

<sup>1</sup>See Ref. [28] Fig. (S2) for the dependence of  $Q$  on  $J/t$  at a fixed filling fraction.

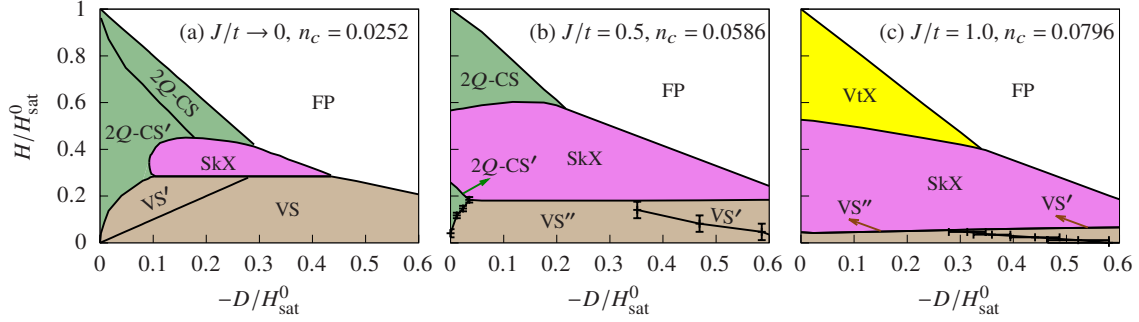


Figure 2: Phase diagrams of the TKLM with easy-axis single-ion anisotropy in a magnetic field with the ordering wave number  $Q = |\mathbf{b}_1|/6$ , where the RKKY limit (a) is taken from Ref. [24]. The error bars of phase boundaries at low field indicate the limited numerical accuracy due to quasi-degenerate states. The saturation field at  $D = 0$  is  $H_{\text{sat}}^0 = 8.53 \times 10^{-4}t$  for (b) and  $H_{\text{sat}}^0 = 4.31 \times 10^{-3}t$  for (c).

Here we employ a variant of the kernel polynomial method (KPM) to obtain an unbiased estimate of the wave vector of low-energy spin configurations [29,30] on finite lattices of  $96 \times 96$  sites. For  $H = D = 0$ ,  $T = 10^{-5}J^2/t$  and  $J/t = \{0.5, 1.0\}$ , we integrate the dimensionless stochastic Landau-Lifshitz (SLL) dynamics with a unit damping parameter using the Heun-projected scheme for a total of 45000 steps of duration  $\Delta\tau = 0.5/(J^2/t)$ . The order of the Chebyshev polynomial expansion is  $M = 1000$  and we use the gradient-based probing method with  $S = 256$  colors [30]. The first 30000 steps are discarded for equilibration and the rest 15000 steps are used for measurements. At each temperature, we average over 6 independent runs to estimate the error bars.

Figures 1(b)-(c) show typical snapshots of the static spin structure factor  $\mathcal{S}(\mathbf{q})$  near the end of the KPM-SLL simulation. For the low filling fractions that we are considering,  $\mathcal{S}(\mathbf{q})$  takes its maximum value on a ring [28]. Note that, in equilibrium, spin configurations with broken discrete symmetries are generally allowed at finite low temperatures [31]. As we will see later, the lack of symmetry breaking in our KPM-SLL simulation is due to the small energy scale of the effective interactions between local moments in units of the bare interactions of the TKLM.

The magnetic unit cell for each filling fraction can be inferred from the  $Q(n_c)$  curve produced by the KPM-SLL simulation, allowing us to exploit the translational symmetry of the optimal spin configuration and find the ground state in the thermodynamic limit. As indicated by the dashed lines of Fig. 1(d), we can always find commensurate ordering wave vectors  $\mathbf{Q}_\nu(n_c)$  by choosing the right filling fraction. For example, for  $Q = |\mathbf{b}_1|/L$ , the magnetic unit cell contains  $L \times L$  spins spanned by the basis  $\{L\mathbf{a}_1, L\mathbf{a}_2\}$ , where  $\mathbf{a}_1$  and  $\mathbf{a}_2$  are primitive vectors of the triangular lattice<sup>2</sup>.

The  $T = 0$  energy density  $e$  of each periodic spin configuration is computed by diagonalizing  $\mathcal{H}$  in momentum space and integrating the sum of energies of occupied single-particle states over the reduced Brillouin zone  $\mathcal{B}_r$ :

$$e = \frac{1}{L^2} \sum_{n=1}^{2L^2} \int_{\mathcal{B}_r} \frac{d\tilde{\mathbf{k}}}{\mathcal{A}_{\mathcal{B}_r}} \Theta[\mu - \epsilon_n(\tilde{\mathbf{k}})] \epsilon_n(\tilde{\mathbf{k}}) + \frac{1}{L^2} \sum_{\mathbf{R}} [-HS_{\mathbf{R}}^z + D(S_{\mathbf{R}}^z)^2], \quad (2)$$

where  $\Theta(x)$  is the Heaviside step function, and  $\mathcal{A}_{\mathcal{B}_r}$  is the area of  $\mathcal{B}_r$ .

<sup>2</sup>For  $J/t \rightarrow 0$ , this becomes identical to the susceptibility analysis in Ref. [24].

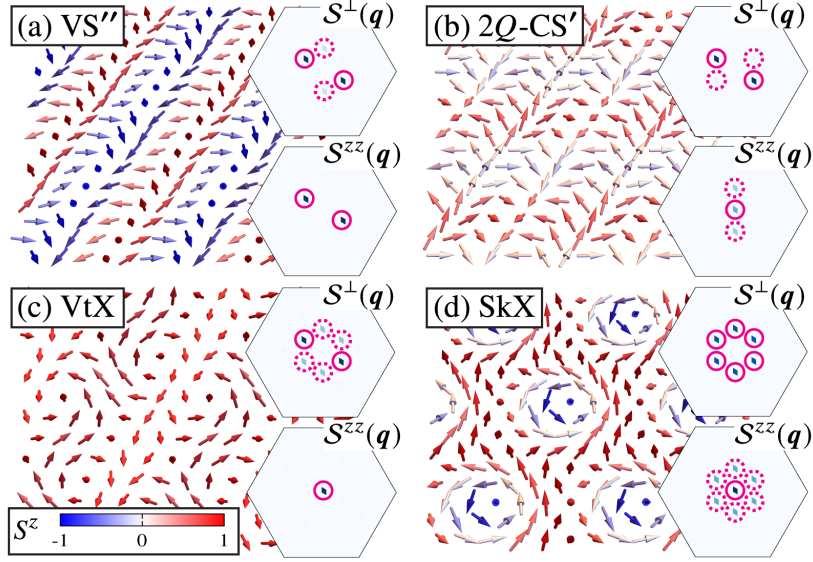


Figure 3: Spin configurations of phases shown in Fig. 2. The insets show the in-plane ( $S^\perp$ ) and out-of-plane ( $S^{zz}$ ) static structure factors in the first Brillouin zone. The solid (dotted) circles highlight the dominant (subdominant) peaks. The spin configurations of VS' and 2Q-CS can be found in Ref. [24].

For convenience, we mainly focus on magnetic orderings with  $L = 6$ <sup>3</sup>, which correspond to  $n_c \approx 0.0586$  for  $J/t = 0.5$  and  $n_c \approx 0.0796$  for  $J/t = 1$  according to Fig. 1. For any fixed parameter set  $\{H, D\}$ , we minimize the energy density  $e$  with respect to  $2L^2$  variational parameters (each  $S_{\mathbf{R}}$  is parametrized by two independent angles) at fixed filling fraction  $n_c$ . To locate the global minimum, we perform many independent runs with different random initial spin configurations (typically 20) and keep only the lowest energy solution (see Appendix A for details).

The results of the variational calculation for  $J/t = \{0.5, 1\}$  are summarized in Fig. 2. In comparison to the weak-coupling regime ( $J/t \ll 1$ ) described by an effective RKKY Hamiltonian [Fig. 2(b) of Ref. [24], reproduced here as Fig. 2(a)], it is clear that the SkX phase expands upon increasing the Kondo coupling. This phenomenon highlights the crucial role played by higher order spin interactions [10, 17]. An important consequence of the strengthening of these interactions is that the single-ion anisotropy is no longer necessary to stabilize the SkX. We have also confirmed that the SkX remains stable for  $J/t = 1$  and  $D = 0$  when the filling fraction is reduced to obtain a smaller ordering wave vector  $Q = |\mathbf{b}_1|/8$  (longer wave length).

In the RKKY limit, we found that the optimal wavevector remains practically unchanged for finite  $D$  and  $H$ , implying that the variational calculation with fixed  $L$  is accurate for the full phase diagram [24]. To verify if this remains true for finite  $J/t$ , we consider a point inside the  $J/t = 0.5$  phase diagram [Fig. 2(b)]:  $H = -2D = 0.469H_{\text{sat}}^0$ . The KPM-SLL simulations indicate that a slightly different filling fraction  $n_c \approx 0.0548$  (the deviation is comparable to the errorbar of the KPM-SLL simulation) is required to keep the ordering wave vector  $Q/|\mathbf{b}_1| = 1/6$  unchanged. The variational calculation for the new filling fraction  $n_c \approx 0.0548$  at  $H = -2D = 0.469H_{\text{sat}}^0$  confirms that the SkX is still the ground state.

Besides further stabilizing the SkX phase, the larger Kondo exchange also produces a few

<sup>3</sup>The choice of commensurate values of  $Q$  is only for the convenience of calculation (nearby incommensurate values of  $Q$  should produce similar phase diagrams).

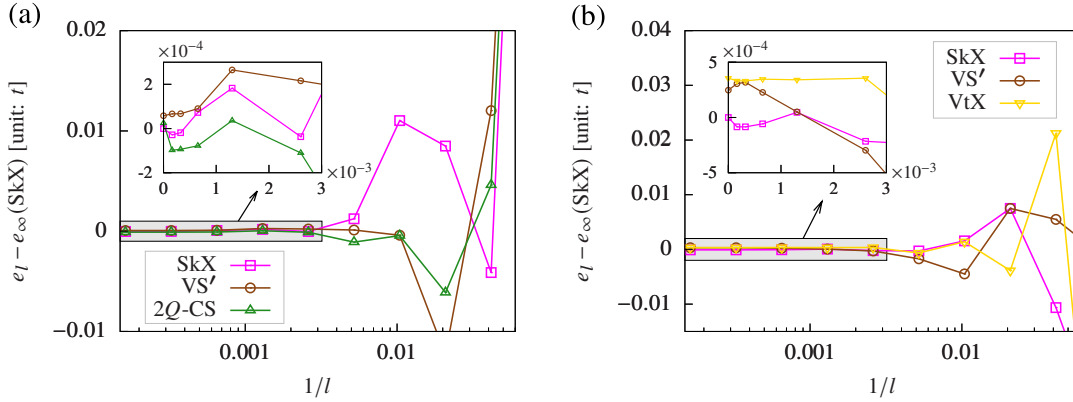


Figure 4: The energy densities  $e_l$  of different states evaluated on a uniform  $(l/L)^2$  mesh in the reduced Brillouin zone  $\mathcal{B}_r$ , shifted by the energy density of the SkX state  $e_\infty(\text{SkX})$  evaluated by the integral Eq. (2). The data points at  $1/l = 0$  are obtained from numerical integration instead of discrete sum. In (a), the three states are obtained by the variational method for the same parameter set  $\{J/t = 0.5, n_c = 0.0586, D/t = -10^{-4}, H/t = 3.125 \times 10^{-4}, L = 6\}$ , converged from different random initial spin configurations; Similarly in (b), the three states are obtained by the variational method for the same parameter set  $\{J/t = 1.0, n_c = 0.0796, D/t = -10^{-3}, H/t = 10^{-3}, L = 6\}$ , converged from different random initial spin configurations. For each parameter set, the SkX state is the ground state in the thermodynamic limit, while the other two states are metastable (local energy minimum).

multi- $Q$  phases that do not appear in the RKKY limit [24]. In particular, a new vertical spiral phase (VS'') [see Fig. 3(a)] and a vortex crystal phase (VtX) [see Fig. 3(c)] appear at low and high fields respectively (see Appendix B for the Fourier analysis of the VS'' and VtX states). We note that the distribution of local scalar spin chirality,  $\mathbf{S}_i \cdot (\mathbf{S}_j \times \mathbf{S}_k)$ , on each triangular plaquette exhibits chiral stripes with alternating signs (zero net scalar chirality) in the VS'', 2Q-CS and 2Q-CS'. Similar stripes of scalar chirality have been reported in Refs. [32, 33]. Vortex crystals below the saturation field have also been reported for spin models with short-range anisotropic exchange interactions [34–36].

To date, there are only two direct numerical confirmations of the SkX ground states in the TKLM (1). The first one is the four-sublattice chiral ordering [8, 29, 37, 38] which is strictly speaking the short wavelength limit ( $L = 2$  and  $Q = |\mathbf{b}_1|/2$ ) of the SkX on a triangular lattice. The second one is directly obtained from the KPM-SLL method by fine-tuning both the third neighbor hopping and the chemical potential [16]. Short wavelength multi- $Q$  chiral spin structures on kagome KLM were also reported with fine-tuned Fermi surfaces [39]. The fine-tuning is required to get sharp peaks of the Lindhard function and maximize the magnitude of the effective spin-spin interactions. It is then natural to ask why previous numerical attempts were not able to identify the ubiquitous nature of 3- $Q$  SkX orderings in the TKLM.

The key observation is that the effective spin interactions (RKKY and higher order terms) are much smaller than the bare coupling constant  $J$ , as it is clear from the values of the saturation fields in Fig. 2 [ $H_{\text{sat}}^0 = 8.53 \times 10^{-4}t$  for (b) and  $H_{\text{sat}}^0 = 4.31 \times 10^{-3}t$  for (c)]. Furthermore, the splitting between competing single and multi- $Q$  orderings is controlled by an even smaller energy scale that results from the competition between effective higher order spin interactions and



the small RKKY energy cost of higher harmonic components of generic multi- $Q$  orderings, which are required to fulfill the normalization constraint  $|\mathcal{S}_i| = 1$ . This situation leads to very small differences of the energy density,  $\Delta e$ , in units of the hopping amplitude  $t$ . Such small energy differences are sensitive to numerical accuracy, which is often limited by system size and by other approximations of the numerical method (e.g., the order of the Chebyshev polynomial expansion and number of random vectors in the KPM-SLL method). To estimate the error introduced by the finite size effects, we simply need to replace the integral in Eq. (2) with a discrete sum on a uniform  $(l/L)^2$  grid in  $\mathcal{B}_r$ . The discrete sum corresponds to the energy density of the given spin configuration on a finite lattice of  $N = l^2$  sites. In Fig. 4(a), we consider three converged spin configurations, corresponding to a stable SkX and metastable  $VS'$  and  $2Q$ -CS solutions obtained with the variational method for the same parameter set and different random initial spin configurations. The dependence of the energy densities on the linear lattice size,  $e_l$ , clearly indicates that for  $J/t = 0.5$  it is necessary to consider finite lattices with  $l \gg 6000$  to obtain results that are representative of the thermodynamic limit. Even For  $J/t = 1$ , Fig. 4(b) shows that a lattice with  $l \gg 1000$  is required to achieve convergence, which is beyond the typical system size that can be reached with the KPM-SLL method. In other words, it is essential to take the thermodynamic limit in Eq. (2) (performing high-accuracy integration) in order to find the correct low energy states of the KLM for general sets of parameters.

### 3 Conclusion

A key outcome of this work is to demonstrate that SkXs are ubiquitous phases of KLMs with hexagonal symmetry, that span a large spectrum of wavelengths ranging from  $\lambda \gg a$  for small Fermi surfaces [24] to the short wave length or dense limit  $\lambda = 2a$  corresponding to the ‘‘tetrahedral’’ ordering reported in Refs. [8, 37, 38]. Based on our results, we conjecture that SkXs of intermediate wave lengths between six and two lattice parameters (e.g.  $\lambda = 4a$ ) should also emerge above a critical value of  $J/t$  for some range of filling fractions between  $n = 0.06$  and  $n = 0.25$ . We also expect SkXs to appear for even higher filling fractions with more complicated Fermi surfaces. In other words, SkXs can emerge without the need of fine tuning the Fermi surface to obtain sharp peaks in the spin susceptibility of the conduction bands. The novel approach that is introduced here avoids this unnecessary complication because the results are directly obtained in the thermodynamic limit. Unlike other approaches in which the magnetic unit cell is fixed in an ad-hoc fashion [37], we have used unbiased numerical simulations to determine the optimal magnetic unit cell for a given filling fraction of the conduction bands.

Establishing a *generic* stabilization mechanism of SkXs in KLMs is very important because most of the known magnetic SkXs have been reported in metals [11–15, 40, 41], where the exchange interaction between magnetic moments and conduction electrons enables novel responses, such as the topological Hall effect (THE) [42–45] and current-induced skyrmion motion [46–49]. The THE arises from the Berry curvature acquired by the reconstructed electronic bands. A crucial distinctive character of the SkXs that emerge in KLMs is that topological Hall effect can be extremely large (comparable to the quantized value) because their lattice spacing is dictated by the Fermi wave vector [13].

The generic nature of the mechanism is particularly relevant because real materials comprise multiple conduction bands and more general forms of Kondo interaction<sup>4</sup>. The key observation

<sup>4</sup>While the variational method introduced in this paper can be straightforwardly applied to more realistic cases, the

is that four and higher-order effective spin interactions generated by processes that involve *independent* pieces of the Fermi surface that are connected by symmetry related wave vectors favor multi- $Q$  spin configurations [see Fig. 1(a)]. While the amplitude of these effective higher order spin interactions cannot be obtained from perturbation theory because they are non-analytic functions of  $J/t$  [9, 10, 16, 18], they can in principle be calculated using other techniques, such as resummation of diagrammatic series. Since their strength relative to the bilinear RKKY interaction grows with  $J/t$ , we expect that, *in absence of easy-axis single-ion anisotropy*, field induced SkXs and other multi- $Q$  orderings should emerge above a critical value of  $J/t$ . This conclusion is supported by an increasing number of experimental results in  $f$ -electron magnets [50–56]. We note that  $d$ -electron systems with localized moments in  $t_{2g}$  orbitals coupled via Hund’s exchange to conduction  $e_g$  electrons can also provide natural realizations of the intermediate-coupling regime  $J \gtrsim t$  considered in this work [57–62].

## Acknowledgements

We thank Shi-Zeng Lin and Kipton Barros for helpful discussions. ZW was supported by funding from the Lincoln Chair of Excellence in Physics. During the writing of this paper, ZW was supported by the U.S. Department of Energy through the University of Minnesota Center for Quantum Materials, under Award No. DE-SC-0016371. CDB acknowledges support from U.S. Department of Energy, Office of Science, Office of Basic Energy Sciences, under Award No. DE-SC0022311. This research used resources of the Oak Ridge Leadership Computing Facility at the Oak Ridge National Laboratory, which is supported by the Office of Science of the U.S. Department of Energy under Contract No. DE-AC05-00OR22725.

## A Variational Method

In this section we consider the  $T = 0$  commensurate states. Furthermore, we assume that the magnetic unit cell is spanned by the basis  $\{L\mathbf{a}_1, L\mathbf{a}_2\}$ , where  $\mathbf{a}_1$  and  $\mathbf{a}_2$  are the primitive vectors of the triangular lattice. Note that the value of  $L$  can be estimated from unbiased techniques, such as the KPM-SLL method [29, 30] used in this paper, which can be implemented in relatively large lattices.

In the following, we will label different sublattices of the magnetic unitcell by  $\mathbf{R}$ , and different unitcells by  $\tilde{\mathbf{r}}$ , so the coordinates of each site can be expressed as the sum  $\mathbf{r} = \tilde{\mathbf{r}} + \mathbf{R}$  [63]. The translational symmetry of these commensurate states allows us to perform the Fourier transform:

$$c_{\tilde{\mathbf{r}}, \mathbf{R}, \sigma} = \sqrt{\frac{L^2}{N}} \sum_{\tilde{\mathbf{k}}} e^{i\tilde{\mathbf{k}} \cdot \tilde{\mathbf{r}}} c_{\tilde{\mathbf{k}}, \mathbf{R}, \sigma}, \quad (3)$$

where  $N$  is the total number of the lattice sites, and  $\tilde{\mathbf{k}}$  labels the allowed momenta in the reduced Brillouin zone  $\mathcal{B}_r$ .

---

enlarged matrix size due to multiple conduction bands poses an additional numerical challenge, which can be alleviated by using modern parallel computing hardware.



The KLM considered in the main text becomes block-diagonal in  $\tilde{\mathbf{k}}$ -space,  $\mathcal{H} = \sum_{\tilde{\mathbf{k}}} \mathcal{H}_{\tilde{\mathbf{k}}}$ , with

$$\mathcal{H}_{\tilde{\mathbf{k}}} = \sum_{\mathbf{R}} \left[ -t \sum_{\eta} \sum_{\sigma} c_{\tilde{\mathbf{k}}, \mathbf{R}, \sigma}^{\dagger} c_{\tilde{\mathbf{k}}, \mathbf{R} + \mathbf{r}_{\eta}, \sigma} + J \sum_{\alpha\beta} c_{\tilde{\mathbf{k}}, \mathbf{R}, \alpha}^{\dagger} \sigma_{\alpha\beta} c_{\tilde{\mathbf{k}}, \mathbf{R}, \beta} \cdot \mathbf{S}_{\mathbf{R}} - HS_{\mathbf{R}}^z + D(S_{\mathbf{R}}^z)^2 \right]. \quad (4)$$

The single-particle eigenstates are obtained by diagonalizing the  $2L^2 \times 2L^2$  block matrix of the operator  $\mathcal{H}_{\tilde{\mathbf{k}}}$  whose eigenvalues are denoted by  $\epsilon_{\tilde{\mathbf{k}}, n}$ .

The energy density at  $T = 0$  can be written as

$$e = \frac{1}{N} \sum_{\tilde{\mathbf{k}}} \sum_{n=1}^{2L^2} \Theta(\mu - \epsilon_{\tilde{\mathbf{k}}, n}) \epsilon_{\tilde{\mathbf{k}}, n} + \frac{1}{L^2} \sum_{\mathbf{R}} [-HS_{\mathbf{R}}^z + D(S_{\mathbf{R}}^z)^2]. \quad (5)$$

While Eq. (5) is valid for any system size, it is crucial to take the thermodynamic limit  $N \rightarrow \infty$  to identify the correct ground state of the KLM. This is done by converting the discrete sum  $\frac{1}{N} \sum_{\tilde{\mathbf{k}}}$  into the integral:

$$e = \frac{1}{L^2} \int_{\mathcal{B}_r} \frac{d\tilde{\mathbf{k}}}{\mathcal{A}_{\mathcal{B}_r}} \sum_{n=1}^{2L^2} \Theta(\mu - \epsilon_{\tilde{\mathbf{k}}, n}) \epsilon_{\tilde{\mathbf{k}}, n} + \frac{1}{L^2} \sum_{\mathbf{R}} [-HS_{\mathbf{R}}^z + D(S_{\mathbf{R}}^z)^2], \quad (6)$$

where  $\mathcal{A}_{\mathcal{B}_r}$  is the area of the reduced Brillouin zone  $\mathcal{B}_r$ . For the canonical ensemble used in this paper, the chemical potential  $\mu$  is determined self-consistently at every step of the minimization from the filling fraction:

$$n_c = \frac{1}{2L^2} \int_{\mathcal{B}_r} \frac{d\tilde{\mathbf{k}}}{\mathcal{A}_{\mathcal{B}_r}} \sum_{n=1}^{2L^2} \Theta(\mu - \epsilon_{\tilde{\mathbf{k}}, n}). \quad (7)$$

The  $T = 0$  states can be obtained by minimizing  $e$  at fixed  $n_c$  as a function of the  $2L^2$  variational parameters corresponding to the two angles that parametrize the state of each classical moment  $\mathbf{S}_{\mathbf{R}}$  [64–66]. For local minimization algorithms, the converged results are often metastable local minima (different initial conditions can lead to different final states). For each parameter set, we typically perform 20 independent runs with different random initial spin configurations.

The combination of exact diagonalization, integration and minimization is computationally expensive. To obtain converged results in reasonable amount of time, it is beneficial to use derivative based minimization algorithms. The derivative of the energy density is given by:

$$\frac{de}{d\mathbf{S}_{\mathbf{R}}} = \frac{1}{L^2} \int_{\mathcal{B}_r} \frac{d\tilde{\mathbf{k}}}{\mathcal{A}_{\mathcal{B}_r}} \text{Tr} \left[ f(\tilde{\mathbf{k}}) \frac{dh(\tilde{\mathbf{k}})}{d\mathbf{S}_{\mathbf{R}}} \right] + \frac{1}{L^2} \left[ -H \begin{pmatrix} 0 \\ 0 \\ 1 \end{pmatrix} + 2D \begin{pmatrix} 0 \\ 0 \\ S_{\mathbf{R}}^z \end{pmatrix} \right], \quad (8)$$

where  $h(\tilde{\mathbf{k}})$  is the  $2L^2 \times 2L^2$  matrix of the operator  $\mathcal{H}_{\tilde{\mathbf{k}}}$  given in Eq. (4),

$$f(\tilde{\mathbf{k}}) = \sum_{n=1}^{2L^2} \Theta(\mu - \epsilon_{\tilde{\mathbf{k}}, n}) |\psi_{\tilde{\mathbf{k}}, n}\rangle \langle \psi_{\tilde{\mathbf{k}}, n}|, \quad (9)$$

is the density matrix, and  $|\psi_{\tilde{\mathbf{k}}, n}\rangle$  is the eigenvector with eigenvalue  $\epsilon_{\tilde{\mathbf{k}}, n}$ .

## B Fourier analysis

For most of the states that appear in this paper, the Fourier analysis has been documented in Ref. [24]. Here we further analyze the new states that appear in the phase diagram for larger values of  $J/t$ .

Denote the ordering wave vectors as

$$\mathbf{Q}_1 = -\mathbf{b}_2/L, \quad \mathbf{Q}_2 = \mathbf{b}_1/L, \quad \mathbf{Q}_3 = -\mathbf{Q}_1 - \mathbf{Q}_2. \quad (10)$$

In the  $VS''$  phase, the normalized spin configurations  $\mathbf{S}_r = \mathbf{m}_r/|\mathbf{m}_r|$  can be parametrized as:

$$m_{r-r_0}^x = -a_1 \cos \phi \sin(\mathbf{Q}_1 \cdot \mathbf{r}) + a_2 \sin \phi \sin(\mathbf{Q}_2 \cdot \mathbf{r}), \quad (11a)$$

$$m_{r-r_0}^y = -a_1 \sin \phi \sin(\mathbf{Q}_1 \cdot \mathbf{r}) - a_2 \cos \phi \sin(\mathbf{Q}_2 \cdot \mathbf{r}), \quad (11b)$$

$$m_{r-r_0}^z = a_0 - a_1 \cos(\mathbf{Q}_1 \cdot \mathbf{r}). \quad (11c)$$

The normalized spin configurations of the VtX phase can be parametrized as:

$$m_{r-r_0}^x = a_1 \sin \phi \sin(\mathbf{Q}_1 \cdot \mathbf{r}) - a_2 \cos \phi [\cos(\mathbf{Q}_2 \cdot \mathbf{r} + \theta) - \cos(\mathbf{Q}_3 \cdot \mathbf{r} + \theta)], \quad (12a)$$

$$m_{r-r_0}^y = a_1 \cos \phi \sin(\mathbf{Q}_1 \cdot \mathbf{r}) + a_2 \sin \phi [\cos(\mathbf{Q}_2 \cdot \mathbf{r} + \theta) - \cos(\mathbf{Q}_3 \cdot \mathbf{r} + \theta)], \quad (12b)$$

$$m_{r-r_0}^z = a_0 - a_3 \sin(\mathbf{Q}_1 \cdot \mathbf{r}). \quad (12c)$$

## References

- [1] A. N. Bogdanov and D. A. Yablonskii, *Thermodynamically stable "vortices" in magnetically ordered crystals: The mixed state of magnets*, Zh. Eksp. Teor. Fiz. **95**, 178 (1989), [Sov. Phys. JETP **68**, 101 (1989)].
- [2] U. K. Rößler, A. N. Bogdanov and C. Pfleiderer, *Spontaneous skyrmion ground states in magnetic metals*, Nature **442**, 797 (2006), doi:[10.1038/nature05056](https://doi.org/10.1038/nature05056).
- [3] S. Mühlbauer, B. Binz, F. Jonietz, C. Pfleiderer, A. Rosch, A. Neubauer, R. Georgii and P. Böni, *Skyrmion Lattice in a Chiral Magnet*, Science **323**, 915 (2009), doi:[10.1126/science.1166767](https://doi.org/10.1126/science.1166767).
- [4] X. Z. Yu, Y. Onose, N. Kanazawa, J. H. Park, J. H. Han, Y. Matsui, N. Nagaosa and Y. Tokura, *Real-space observation of a two-dimensional skyrmion crystal*, Nature **465**, 901 (2010), doi:[10.1038/nature09124](https://doi.org/10.1038/nature09124).
- [5] X. Z. Yu, N. Kanazawa, Y. Onose, K. Kimoto, W. Z. Zhang, S. Ishiwata, Y. Matsui and Y. Tokura, *Near room-temperature formation of a skyrmion crystal in thin-films of the helimagnet FeGe*, Nat. Mater. **10**, 106 (2011), doi:[10.1038/nmat2916](https://doi.org/10.1038/nmat2916).
- [6] S. Seki, X. Z. Yu, S. Ishiwata and Y. Tokura, *Observation of skyrmions in a multiferroic material*, Science **336**, 198 (2012), doi:[10.1126/science.1214143](https://doi.org/10.1126/science.1214143).
- [7] T. Adams, A. Chacon, M. Wagner, A. Bauer, G. Brandl, B. Pedersen, H. Berger, P. Lemmens and C. Pfleiderer, *Long-Wavelength Helimagnetic Order and Skyrmion Lattice Phase in  $\text{Cu}_2\text{OSeO}_3$* , Phys. Rev. Lett. **108**, 237204 (2012), doi:[10.1103/PhysRevLett.108.237204](https://doi.org/10.1103/PhysRevLett.108.237204).

- [8] I. Martin and C. D. Batista, *Itinerant electron-driven chiral magnetic ordering and spontaneous quantum hall effect in triangular lattice models*, Phys. Rev. Lett. **101**, 156402 (2008), doi:[10.1103/PhysRevLett.101.156402](https://doi.org/10.1103/PhysRevLett.101.156402).
- [9] Y. Akagi, M. Udagawa and Y. Motome, *Hidden Multiple-Spin Interactions as an Origin of Spin Scalar Chiral Order in Frustrated Kondo Lattice Models*, Phys. Rev. Lett. **108**, 096401 (2012), doi:[10.1103/PhysRevLett.108.096401](https://doi.org/10.1103/PhysRevLett.108.096401).
- [10] C. D. Batista, S.-Z. Lin, S. Hayami and Y. Kamiya, *Frustration and chiral orderings in correlated electron systems*, Rep. Prog. Phys. **79**, 084504 (2016), doi:[10.1088/0034-4885/79/8/084504](https://doi.org/10.1088/0034-4885/79/8/084504).
- [11] R. Mallik, E. V. Sampathkumaran, P. L. Paulose, H. Sugawara and H. Sato, *Magnetic anomalies in  $Gd_2PdSi_3$* , Pramana - J. Phys. **51**, 505 (1998), doi:[10.1007/BF02828942](https://doi.org/10.1007/BF02828942).
- [12] S. R. Saha, H. Sugawara, T. D. Matsuda, H. Sato, R. Mallik and E. V. Sampathkumaran, *Magnetic anisotropy, first-order-like metamagnetic transitions, and large negative magnetoresistance in single-crystal  $Gd_2PdSi_3$* , Phys. Rev. B **60**, 12162 (1999), doi:[10.1103/PhysRevB.60.12162](https://doi.org/10.1103/PhysRevB.60.12162).
- [13] T. Kurumaji, T. Nakajima, M. Hirschberger, A. Kikkawa, Y. Yamasaki, H. Sagayama, H. Nakao, Y. Taguchi, T.-h. Arima and Y. Tokura, *Skyrmion lattice with a giant topological Hall effect in a frustrated triangular-lattice magnet*, Science **365**, 914 (2019), doi:[10.1126/science.aau0968](https://doi.org/10.1126/science.aau0968).
- [14] V. Chandragiri, K. K. Iyer and E. V. Sampathkumaran, *Magnetic behavior of  $Gd_3Ru_4Al_{12}$ , a layered compound with distorted kagomé net*, J. Phys.: Condens. Matter **28**, 286002 (2016), doi:[10.1088/0953-8984/28/28/286002](https://doi.org/10.1088/0953-8984/28/28/286002).
- [15] M. Hirschberger, T. Nakajima, S. Gao, L. Peng, A. Kikkawa, T. Kurumaji, M. Kriener, Y. Yamasaki, H. Sagayama, H. Nakao, K. Ohishi, K. Kakurai *et al.*, *Skyrmion phase and competing magnetic orders on a breathing kagomé lattice*, Nat. Commun. **10**, 5831 (2019), doi:[10.1038/s41467-019-13675-4](https://doi.org/10.1038/s41467-019-13675-4).
- [16] R. Ozawa, S. Hayami and Y. Motome, *Zero-field skyrmions with a high topological number in itinerant magnets*, Phys. Rev. Lett. **118**, 147205 (2017), doi:[10.1103/PhysRevLett.118.147205](https://doi.org/10.1103/PhysRevLett.118.147205).
- [17] S. Hayami and Y. Motome, *Topological spin crystals by itinerant frustration*, J. Phys.: Condens. Matter **33**, 443001 (2021), doi:[10.1088/1361-648X/ac1a30](https://doi.org/10.1088/1361-648X/ac1a30).
- [18] S. Hayami, R. Ozawa and Y. Motome, *Effective bilinear-biquadratic model for noncoplanar ordering in itinerant magnets*, Phys. Rev. B **95**, 224424 (2017), doi:[10.1103/PhysRevB.95.224424](https://doi.org/10.1103/PhysRevB.95.224424).
- [19] S. Heinze, K. von Bergmann, M. Menzel, J. Brede, A. Kubetzka, R. Wiesendanger, G. Bihlmayer and S. Blügel, *Spontaneous atomic-scale magnetic skyrmion lattice in two dimensions*, Nat. Phys. **7**, 713 (2011), doi:[10.1038/nphys2045](https://doi.org/10.1038/nphys2045).
- [20] S. Kumar and J. van den Brink, *Frustration-induced insulating chiral spin state in itinerant triangular-lattice magnets*, Phys. Rev. Lett. **105**, 216405 (2010), doi:[10.1103/PhysRevLett.105.216405](https://doi.org/10.1103/PhysRevLett.105.216405).

- [21] S. Reja, R. Ray, J. van den Brink and S. Kumar, *Coupled spin-charge order in frustrated itinerant triangular magnets*, Phys. Rev. B **91**, 140403 (2015), doi:[10.1103/PhysRevB.91.140403](https://doi.org/10.1103/PhysRevB.91.140403).
- [22] D. S. Kathyat, A. Mukherjee and S. Kumar, *Microscopic magnetic Hamiltonian for exotic spin textures in metals*, Phys. Rev. B **102**, 075106 (2020), doi:[10.1103/PhysRevB.102.075106](https://doi.org/10.1103/PhysRevB.102.075106).
- [23] D. S. Kathyat, A. Mukherjee and S. Kumar, *Electronic mechanism for nanoscale skyrmions and topological metals*, Phys. Rev. B **103**, 035111 (2021), doi:[10.1103/PhysRevB.103.035111](https://doi.org/10.1103/PhysRevB.103.035111).
- [24] Z. Wang, Y. Su, S.-Z. Lin and C. D. Batista, *Skyrmion crystal from RKKY interaction mediated by 2D electron gas*, Phys. Rev. Lett. **124**, 207201 (2020), doi:[10.1103/PhysRevLett.124.207201](https://doi.org/10.1103/PhysRevLett.124.207201).
- [25] M. A. Ruderman and C. Kittel, *Indirect Exchange Coupling of Nuclear Magnetic Moments by Conduction Electrons*, Phys. Rev. **96**, 99 (1954), doi:[10.1103/PhysRev.96.99](https://doi.org/10.1103/PhysRev.96.99).
- [26] T. Kasuya, *A Theory of Metallic Ferro- and Antiferromagnetism on Zener's Model*, Prog. Theor. Phys. **16**, 45 (1956), doi:[10.1143/PTP.16.45](https://doi.org/10.1143/PTP.16.45).
- [27] K. Yosida, *Magnetic Properties of Cu-Mn Alloys*, Phys. Rev. **106**, 893 (1957), doi:[10.1103/PhysRev.106.893](https://doi.org/10.1103/PhysRev.106.893).
- [28] Z. Wang, K. Barros, G.-W. Chern, D. L. Maslov and C. D. Batista, *Resistivity minimum in highly frustrated itinerant magnets*, Phys. Rev. Lett. **117**, 206601 (2016), doi:[10.1103/PhysRevLett.117.206601](https://doi.org/10.1103/PhysRevLett.117.206601).
- [29] K. Barros and Y. Kato, *Efficient Langevin simulation of coupled classical fields and fermions*, Phys. Rev. B **88**, 235101 (2013), doi:[10.1103/PhysRevB.88.235101](https://doi.org/10.1103/PhysRevB.88.235101).
- [30] Z. Wang, G.-W. Chern, C. D. Batista and K. Barros, *Gradient-based stochastic estimation of the density matrix*, J. Chem. Phys. **148**, 094107 (2018), doi:[10.1063/1.5017741](https://doi.org/10.1063/1.5017741).
- [31] T. Okubo, S. Chung and H. Kawamura, *Multiple- $q$  States and the Skyrmion Lattice of the Triangular-Lattice Heisenberg Antiferromagnet under Magnetic Fields*, Phys. Rev. Lett. **108**, 017206 (2012), doi:[10.1103/PhysRevLett.108.017206](https://doi.org/10.1103/PhysRevLett.108.017206).
- [32] D. Solenov, D. Mozyrsky and I. Martin, *Chirality Waves in Two-Dimensional Magnets*, Phys. Rev. Lett. **108**, 096403 (2012), doi:[10.1103/PhysRevLett.108.096403](https://doi.org/10.1103/PhysRevLett.108.096403).
- [33] R. Ozawa, S. Hayami, K. Barros, G.-W. Chern, Y. Motome and C. D. Batista, *Vortex crystals with chiral stripes in itinerant magnets*, J. Phys. Soc. Jpn. **85**, 103703 (2016), doi:[10.7566/JPSJ.85.103703](https://doi.org/10.7566/JPSJ.85.103703).
- [34] Y. Kamiya and C. D. Batista, *Magnetic vortex crystals in frustrated mott insulator*, Phys. Rev. X **4**, 011023 (2014), doi:[10.1103/PhysRevX.4.011023](https://doi.org/10.1103/PhysRevX.4.011023).
- [35] Z. Wang, Y. Kamiya, A. H. Nevidomskyy and C. D. Batista, *Three-dimensional crystallization of vortex strings in frustrated quantum magnets*, Phys. Rev. Lett. **115**, 107201 (2015), doi:[10.1103/PhysRevLett.115.107201](https://doi.org/10.1103/PhysRevLett.115.107201).
- [36] Z. Wang, Y. Su, S.-Z. Lin and C. D. Batista, *Meron, skyrmion, and vortex crystals in centrosymmetric tetragonal magnets*, Phys. Rev. B **103**, 104408 (2021), doi:[10.1103/PhysRevB.103.104408](https://doi.org/10.1103/PhysRevB.103.104408).

- [37] Y. Akagi and Y. Motome, *Spin Chirality Ordering and Anomalous Hall Effect in the Ferromagnetic Kondo Lattice Model on a Triangular Lattice*, J. Phys. Soc. Jpn. **79**, 083711 (2010), doi:[10.1143/JPSJ.79.083711](https://doi.org/10.1143/JPSJ.79.083711).
- [38] Y. Kato, I. Martin and C. D. Batista, *Stability of the spontaneous quantum hall state in the triangular kondo-lattice model*, Phys. Rev. Lett. **105**, 266405 (2010), doi:[10.1103/PhysRevLett.105.266405](https://doi.org/10.1103/PhysRevLett.105.266405).
- [39] K. Barros, J. W. F. Venderbos, G.-W. Chern and C. D. Batista, *Exotic magnetic orderings in the kagome Kondo-lattice model*, Phys. Rev. B **90**, 245119 (2014), doi:[10.1103/PhysRevB.90.245119](https://doi.org/10.1103/PhysRevB.90.245119).
- [40] X. Yu, M. Mostovoy, Y. Tokunaga, W. Zhang, K. Kimoto, Y. Matsui, Y. Kaneko, N. Nagaosa and Y. Tokura, *Magnetic stripes and skyrmions with helicity reversals*, PNAS **109**, 8856 (2012), doi:[10.1073/pnas.1118496109](https://doi.org/10.1073/pnas.1118496109).
- [41] X. Z. Yu, Y. Tokunaga, Y. Kaneko, W. Z. Zhang, K. Kimoto, Y. Matsui, Y. Taguchi and Y. Tokura, *Biskyrmion states and their current-driven motion in a layered manganite*, Nat. Commun. **5**, 3198 (2014), doi:[10.1038/ncomms4198](https://doi.org/10.1038/ncomms4198).
- [42] M. Onoda, G. Tatara and N. Nagaosa, *Anomalous hall effect and skyrmion number in real and momentum spaces*, J. Phys. Soc. Jpn. **73**, 2624 (2004), doi:[10.1143/JPSJ.73.2624](https://doi.org/10.1143/JPSJ.73.2624).
- [43] S. D. Yi, S. Onoda, N. Nagaosa and J. H. Han, *Skyrmions and anomalous Hall effect in a Dzyaloshinskii-Moriya spiral magnet*, Phys. Rev. B **80**, 054416 (2009), doi:[10.1103/PhysRevB.80.054416](https://doi.org/10.1103/PhysRevB.80.054416).
- [44] K. Hamamoto, M. Ezawa and N. Nagaosa, *Quantized topological Hall effect in skyrmion crystal*, Phys. Rev. B **92**, 115417 (2015), doi:[10.1103/PhysRevB.92.115417](https://doi.org/10.1103/PhysRevB.92.115417).
- [45] B. Göbel, A. Mook, J. Henk and I. Mertig, *Unconventional topological Hall effect in skyrmion crystals caused by the topology of the lattice*, Phys. Rev. B **95**, 094413 (2017), doi:[10.1103/PhysRevB.95.094413](https://doi.org/10.1103/PhysRevB.95.094413).
- [46] F. Jonietz, S. Mühlbauer, C. Pfleiderer, A. Neubauer, W. Münzer, A. Bauer, T. Adams, R. Georgii, P. Böni, R. A. Duine, K. Everschor, M. Garst *et al.*, *Spin Transfer Torques in MnSi at Ultralow Current Densities*, Science **330**, 1648 (2010), doi:[10.1126/science.1195709](https://doi.org/10.1126/science.1195709).
- [47] X. Z. Yu, N. Kanazawa, W. Z. Zhang, T. Nagai, T. Hara, K. Kimoto, Y. Matsui, Y. Onose and Y. Tokura, *Skyrmion flow near room temperature in an ultralow current density*, Nat. Commun. **3**, 988 (2012), doi:[10.1038/ncomms1990](https://doi.org/10.1038/ncomms1990).
- [48] T. Schulz, R. Ritz, A. Bauer, M. Halder, M. Wagner, C. Franz, C. Pfleiderer, K. Everschor, M. Garst and A. Rosch, *Emergent electrodynamics of skyrmions in a chiral magnet*, Nat. Phys. **8**, 301 (2012), doi:[10.1038/nphys2231](https://doi.org/10.1038/nphys2231).
- [49] N. Nagaosa and Y. Tokura, *Topological properties and dynamics of magnetic skyrmions*, Nat. Nanotechnol. **8**, 899 (2013), doi:[10.1038/nnano.2013.243](https://doi.org/10.1038/nnano.2013.243).
- [50] N. D. Khanh, T. Nakajima, X. Yu, S. Gao, K. Shibata, M. Hirschberger, Y. Yamasaki, H. Sagayama, H. Nakao, L. Peng, K. Nakajima, R. Takagi *et al.*, *Nanometric square skyrmion lattice in a centrosymmetric tetragonal magnet*, Nat. Nanotechnol. **15**, 444 (2020), doi:[10.1038/s41565-020-0684-7](https://doi.org/10.1038/s41565-020-0684-7).

- [51] T. Shang, Y. Xu, D. J. Gawryluk, J. Z. Ma, T. Shiroka, M. Shi and E. Pomjakushina, *Anomalous Hall resistivity and possible topological Hall effect in the  $\text{EuAl}_4$  antiferromagnet*, Phys. Rev. B **103**, L020405 (2021), doi:[10.1103/PhysRevB.103.L020405](https://doi.org/10.1103/PhysRevB.103.L020405).
- [52] Y. Xu, L. Das, J. Z. Ma, C. J. Yi, S. M. Nie, Y. G. Shi, A. Tiwari, S. S. Tsirkin, T. Neupert, M. Medarde, M. Shi, J. Chang *et al.*, *Unconventional Transverse Transport above and below the Magnetic Transition Temperature in Weyl Semimetal  $\text{EuCd}_2\text{As}_2$* , Phys. Rev. Lett. **126**, 076602 (2021), doi:[10.1103/PhysRevLett.126.076602](https://doi.org/10.1103/PhysRevLett.126.076602).
- [53] S. Seo, S. Hayami, Y. Su, S. M. Thomas, F. Ronning, E. D. Bauer, J. D. Thompson, S.-Z. Lin and P. F. S. Rosa, *Spin-texture-driven electrical transport in multi-Q antiferromagnets*, Commun. Phys. **4**, 1 (2021), doi:[10.1038/s42005-021-00558-8](https://doi.org/10.1038/s42005-021-00558-8).
- [54] K. Kaneko, T. Kawasaki, A. Nakamura, K. Munakata, A. Nakao, T. Hanashima, R. Kiyonagi, T. Ohhara, M. Hedo, T. Nakama and Y. Ōnuki, *Charge-Density-Wave Order and Multiple Magnetic Transitions in Divalent Europium Compound  $\text{EuAl}_4$* , J. Phys. Soc. Jpn. **90**, 064704 (2021), doi:[10.7566/JPSJ.90.064704](https://doi.org/10.7566/JPSJ.90.064704).
- [55] H. Zhang, X. Y. Zhu, Y. Xu, D. J. Gawryluk, W. Xie, S. L. Ju, M. Shi, T. Shiroka, Q. F. Zhan, E. Pomjakushina and T. Shang, *Giant magnetoresistance and topological Hall effect in the  $\text{EuGa}_4$  antiferromagnet*, J. Phys.: Condens. Matter **34**, 034005 (2021), doi:[10.1088/1361-648X/ac3102](https://doi.org/10.1088/1361-648X/ac3102).
- [56] J. M. Moya, S. Lei, E. M. Clements, C. S. Kengle, S. Sun, K. Allen, Q. Li, Y. Y. Peng, A. A. Husain, M. Mitrano, M. J. Krogstad, R. Osborn *et al.*, *Incommensurate magnetic orders and topological Hall effect in the square-net centrosymmetric  $\text{EuGa}_2\text{Al}_2$  system*, Phys. Rev. Materials **6**, 074201 (2022), doi:[10.1103/PhysRevMaterials.6.074201](https://doi.org/10.1103/PhysRevMaterials.6.074201).
- [57] W. Wang, Y. Zhang, G. Xu, L. Peng, B. Ding, Y. Wang, Z. Hou, X. Zhang, X. Li, E. Liu, S. Wang, J. Cai *et al.*, *A Centrosymmetric Hexagonal Magnet with Superstable Biskyrmion Magnetic Nanodomains in a Wide Temperature Range of 100–340 K*, Advanced Materials **28**, 6887 (2016), doi:[10.1002/adma.201600889](https://doi.org/10.1002/adma.201600889).
- [58] H. Li, B. Ding, J. Chen, Z. Li, Z. Hou, E. Liu, H. Zhang, X. Xi, G. Wu and W. Wang, *Large topological Hall effect in a geometrically frustrated kagome magnet  $\text{Fe}_3\text{Sn}_2$* , Appl. Phys. Lett. **114**, 192408 (2019), doi:[10.1063/1.5088173](https://doi.org/10.1063/1.5088173).
- [59] S. Wang, Q. Zeng, D. Liu, H. Zhang, L. Ma, G. Xu, Y. Liang, Z. Zhang, H. Wu, R. Che, X. Han and Q. Huang, *Giant Topological Hall Effect and Superstable Spontaneous Skyrmions below 330 K in a Centrosymmetric Complex Noncollinear Ferromagnet  $\text{NdMn}_2\text{Ge}_2$* , ACS Appl. Mater. Interfaces **12**, 24125 (2020), doi:[10.1021/acsami.0c04632](https://doi.org/10.1021/acsami.0c04632).
- [60] X. Zheng, X. Zhao, J. Qi, X. Luo, S. Ma, C. Chen, H. Zeng, G. Yu, N. Fang, S. U. Rehman, W. Ren, B. Li *et al.*, *Giant topological Hall effect around room temperature in noncollinear ferromagnet  $\text{NdMn}_2\text{Ge}_2$  single crystal*, Appl. Phys. Lett. **118**, 072402 (2021), doi:[10.1063/5.0033379](https://doi.org/10.1063/5.0033379).
- [61] R. L. Dally, J. W. Lynn, N. J. Ghimire, D. Michel, P. Siegfried and I. I. Mazin, *Chiral properties of the zero-field spiral state and field-induced magnetic phases of the itinerant kagome metal  $\text{YMn}_6\text{Sn}_6$* , Phys. Rev. B **103**, 094413 (2021), doi:[10.1103/PhysRevB.103.094413](https://doi.org/10.1103/PhysRevB.103.094413).



- [62] M. R. U. Nabi, A. Wegner, F. Wang, Y. Zhu, Y. Guan, A. Fereidouni, K. Pandey, R. Basnet, G. Acharya, H. O. H. Churchill, Z. Mao and J. Hu, *Giant topological Hall effect in centrosymmetric tetragonal  $Mn_{2-x}Zn_xSb$* , Phys. Rev. B **104**, 174419 (2021), doi:[10.1103/PhysRevB.104.174419](https://doi.org/10.1103/PhysRevB.104.174419).
- [63] D. Sénéchal, *An introduction to quantum cluster methods* <http://arxiv.org/abs/0806.2690>.
- [64] S. G. Johnson, *The nlopt nonlinear-optimization package* <http://github.com/stevengj/nlopt>.
- [65] J. Nocedal, *Updating quasi-Newton matrices with limited storage*, Math. Comp. **35**, 773 (1980), doi:[10.1090/S0025-5718-1980-0572855-7](https://doi.org/10.1090/S0025-5718-1980-0572855-7).
- [66] D. C. Liu and J. Nocedal, *On the limited memory BFGS method for large scale optimization*, Mathematical Programming **45**, 503 (1989), doi:[10.1007/BF01589116](https://doi.org/10.1007/BF01589116).